

Thermal decomposition of precursors and iron oxide properties

Influence of promoters (Mn and Cu) and preparation method

Dalila dos Santos Monteiro¹ · Marluce Oliveira da Guarda Souza¹

Received: 14 December 2014 / Accepted: 3 June 2015 / Published online: 24 June 2015
© Akadémiai Kiadó, Budapest, Hungary 2015

Abstract In this work, manganese and copper promoter effect was investigated over iron oxide obtained by thermal decomposition of iron(III) hydroxoacetate (nominal ratio Fe/Mn = 10 and Fe/Cu = 10). The solids were characterized by X-ray fluorescence, thermal analysis (TG, DTG, DTA), Fourier transform infrared spectroscopy (FTIR), physisorption experiments, thermoprogrammed reduction and powder X-ray diffraction. During the precursor thermal decomposition process, the step referred as dehydration/dehydroxylation was controlled by volatile species diffusion. Decomposition stage [Fe(III) to Fe(II) reduction] was controlled by solid geometry and particle size (Coats–Redfern model). FCA-C sample showed Fe(II)/Fe(III) the highest ratio, indicating that through precursor decomposition process reduction is favored. With the use of Ozawa and Kinssinger methods, it became clear that FMCA precursor decomposition showed the lowest activation energy value leading to solid FMCA-C with higher specific surface area and pore volume than the iron oxide-free dopants. The FMCA-C sample reduces hematite to magnetite (low temperature) easily and shows the highest stability of magnetite under reductive conditions.

Keywords Iron(III) hydroxoacetate · Magnetite · HTS catalyst

Introduction

Iron oxides are important materials under scientific and technological perspective due to their magnetic, electrical, physical, chemical and morphological properties. Among several application fields, those which have lured much interest from researchers are adsorption and catalysis [1, 2].

Different phases of iron oxides are used in catalysis, such as hematite (α -Fe₂O₃) and magnetite (Fe₃O₄), respectively the commercial catalyst and the active phase employed on the carbon monoxide high-temperature shift (HTS) reaction. The catalyst properties can be optimized through incorporation of promoters to the system. Chrome, copper, manganese, magnesium, vanadium and aluminum are among the most employed metals used as promoters [2, 3].

The work of promoters depends significantly on the preparation method. Aspects such as the form of incorporation, for example, coprecipitation or precipitation of iron oxide with subsequent gel impregnation using the promoter salt solution, influence the metal dispersion as well as catalytic properties [3, 4]. The nature of the promoter anion salt is also an important parameter, and it can change the precursor thermal decomposition process resulting in altered properties.

The effect of the anion nature in obtaining iron oxides was shown by Rangel [5]. In this study, iron oxide was obtained by decomposition of iron(III) hydroxoacetate, Fe(CH₃COOH)₂(OH), an iron(III) basic acetate, formed by the adsorption of acetate ions in the iron(III) oxyhydroxide gel. The decomposition of iron(III) hydroxoacetate at temperatures ranging between 473 and 673 K in an inert atmosphere generates gaseous products (acetic acid, acetone and carbon monoxide) within the solid, producing reductive atmosphere which favors the formation of magnetite crystalline with higher specific area [5].

✉ Marluce Oliveira da Guarda Souza
mosouza@uneb.br

¹ Departamento de Ciências Exatas e da Terra, Universidade do Estado da Bahia, Rua Silveira Martins, 2555, Cabula, Salvador, Bahia CEP 41.195.001, Brazil

Based on the information above, the decomposition process of iron precursors doped with copper and manganese was studied in this paper. The iron oxide precursors were obtained by coprecipitation of iron and/or manganese hydroxides, followed by gel impregnation with copper nitrate or acetate, in order to evaluate the doping and copper salt anion effects considering kinetic aspects. The structure and properties of materials obtained in the decomposition process were evaluated. The reduction of hematite to magnetite and the stability of magnetite were also studied.

Experimental

Sample preparation

The iron oxide precursors, pure or doped with manganese, were prepared by coprecipitation method, while copper was added to the system by impregnation. Fe/M nominal ratio ($M = \text{Cu}$ and Mn) equals 10 [5].

During coprecipitation, iron nitrate solution ($\text{Fe}(\text{NO}_3)_3 \cdot 9\text{H}_2\text{O}$) (1 mol L^{-1}), manganese nitrate ($\text{Mn}(\text{NO}_3)_3 \cdot 4\text{H}_2\text{O}$) (1 mol L^{-1}) and precipitant potassium hydroxide (KOH) (6 mol L^{-1}) were added simultaneously under stirring to a beaker containing 500 mL ultrapure water. The pH was adjusted to 10 with potassium hydroxide solution at the end of procedure, keeping the system under stirring for 30 min at room temperature for crystals maturation. The system was centrifuged (250 rpm, 5 min), and the gel was rinsed [4 times with ultrapure water and 4 times with ammonium acetate solution 5 % (v/v)]. After each rinsing, the gel was centrifuged. Sample code FM: iron(III) hydroxoacetate doped with Mn.

Precursor pure iron oxide was obtained using the same method. Sample code F: [iron(III) hydroxoacetate].

The gel produced by coprecipitation (FM) was then impregnated with copper(II) nitrate, $\text{Cu}(\text{NO}_3)_2 \cdot 3\text{H}_2\text{O}$, or copper(II) acetate, $\text{Cu}(\text{CH}_3\text{COO})_2 \cdot \text{H}_2\text{O}$, solution (1 mol L^{-1}) for 4 h. Then, it was centrifuged (250 rpm, 5 min) and dried (393 K, 12 h). The solid was ground, sieved

to 80 mesh and calcined at 500 K (2 h, N_2 flow). Sample code FMCN: iron(III) hydroxoacetate doped with Mn and Cu (precursor copper nitrate) and FMCA: iron(III) hydroxoacetate doped with Mn and Cu (precursor copper acetate).

The gel iron(III) hydroxoacetate (F) was also impregnated with copper(II) nitrate, $\text{Cu}(\text{NO}_3)_2 \cdot 3\text{H}_2\text{O}$, or copper(II) acetate, $\text{Cu}(\text{CH}_3\text{COO})_2 \cdot \text{H}_2\text{O}$, solution (1 mol L^{-1}) following the same methodology cited. Sample code FCN: iron(III) hydroxoacetate doped with Cu (precursor copper nitrate) and FCA: iron(III) hydroxoacetate doped with Cu (precursor copper acetate).

The samples after calcination received the following codes: FC; FM-C; FCN-C; FMCN-C; FCA-C and FMCA-C.

Sample characterization

The Fe/Mn and Fe/Cu molar ratios were determined by X-ray fluorescence (XRF) analysis in a Shimadzu model XRF-1800 device, equipped with X-ray tube target with rhodium (4.0 kW). Tablets were made by sample dilution with boric acid (0.15 g acid + 0.15 g sample) and analyzed without pretreatment.

Analyses of Fe(II) were carried out by the dissolution of samples in hydrochloric acid, under a carbon dioxide atmosphere; titration was carried out with a solution of potassium dichromate using diphenylamine as indicator.

Thermogravimetric analysis (TG) and differential thermal analysis (DTA) curves of the iron oxide samples not calcined (10 mg, platinum crucible) were obtained by a Shimadzu DTG-60H thermobalance from 303 to 1273 K at a heating rate of 283 K min^{-1} under nitrogen flow at 30 mL min^{-1} .

The Fourier transform infrared spectroscopy (FTIR) spectra were obtained using a Perkin Elmer equipment model spectrum 100S. The pellets were prepared according to the following mass ratio: 2 mg sample per 200 mg potassium bromide (KBr). Each spectrum was obtained in the region $4000\text{--}400 \text{ cm}^{-1}$ with resolution 4 cm^{-1} .

Shimadzu XRD-6000 diffractometer equipped with a nickel filter and $\text{CuK}\alpha$ radiation (1.5418 \AA) was used in the X-ray diffraction (XRD) experiments. The tube power was 40 kV and 30 mA. The goniometer scanning velocity was 2° min^{-1} (2θ) with 2θ from 10° to 80° . All diffractograms were compared with data sheets from Joint Committee on Power Diffraction Standards (JCPDS) database.

The experiments for determining specific surface area were carried out in a Micrometrics ASAP 2020 equipment. Around 0.25 g of the sample was treated at 473 K under vacuum for 2 h. The physisorption experiments were carried out at 75 K.

The thermoprogrammed reduction (TPR) measurements were taken by 2705 Micromeritics Pulse ChemSorb,

Table 1 Composition of iron oxide doped with manganese and copper. Fe/Mn (mol/mol)

Sample	Fe/Mn	Fe/Cu	Fe(II)/Fe(III)
F-C	–	–	0.30
FM-C	13	–	0.33
FCN-C	–	12	0.33
FMCN-C	13	13	0.32
FCA-C	–	13	0.43
FMCA-C	13	13	0.34

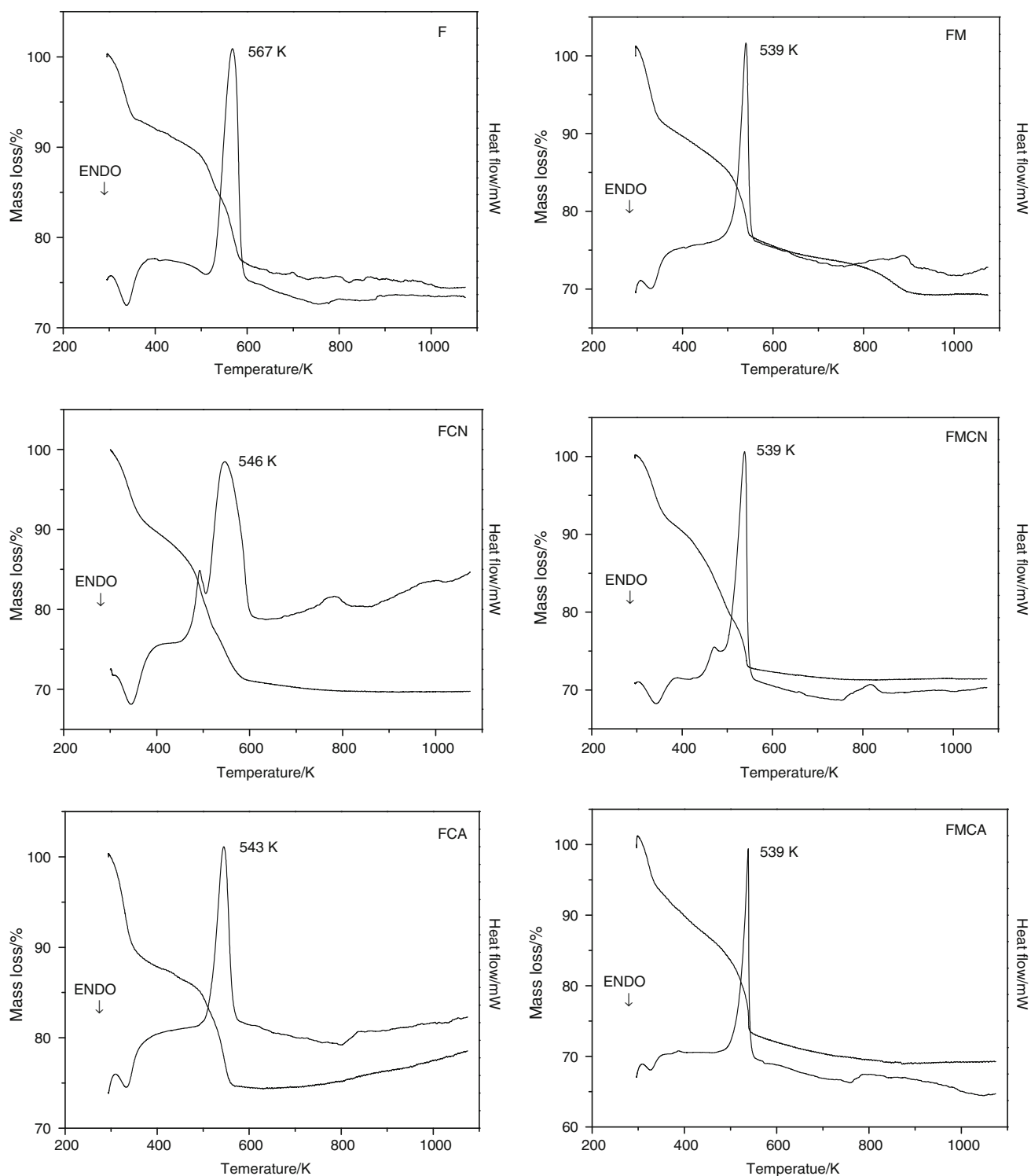


Fig. 1 TG and DTA curves for samples F, FM, FCN, FMCN, FCA and FMCA

equipped with a thermal conductivity detector (TCD). In each analysis, approximately 0.30 g of sample was used, packed into a quartz cell. Prior to analysis, samples were heated at a rate of 283 K min^{-1} under nitrogen flow (60 mL min^{-1}) to 433 K for 30 min and subsequently

cooled to 308 K . For conducting the experiment under reductive conditions, the same amount of sample was subjected to a reducing atmosphere of $5 \% \text{ H}_2/\text{N}_2$ at 30 mL min^{-1} flow rate and 283 K min^{-1} heating rate at 1273 K .

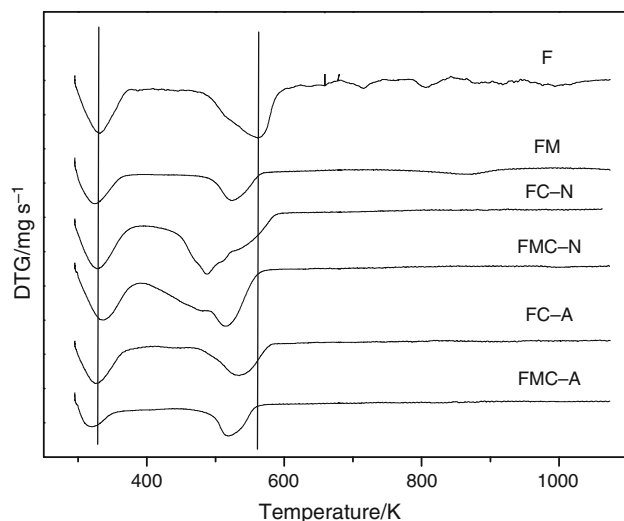


Fig. 2 DTG curve

Results and discussion

Fe/Mn and Fe/Cu solid molar ratios (Table 1) show that the synthesis conditions were favorable to obtaining the solid with the proposed chemical composition. Fe(II)/Fe(III) solid ratio (Table 1) was lower than 0.50, the stoichiometric magnetite value [5]. It may show more than one phase in the oxides produced.

The precursor thermal decomposition was followed by thermoanalytical techniques (TG, DTG and DTA). Two mass loss events were observed in all cases (Fig. 1), the first one with 8–10 % mass loss below 373 K associated with dehydration and/or iron(III) oxyhydroxide dehydroxylation [7]. The second mass loss, at around 523 K ranging from 13 to 17 %, may be associated with the thermal decomposition of the acetate present in the precursor. In these processes, gaseous products are generated, such as acetone, acetic acid and carbon monoxide, which promote the reduction of Fe(III) to Fe(II) ion, with the possible formation of magnetite [5].

In all cases, DTA curve (Fig. 1) showed an endothermic peak at the same temperature range for the first mass loss event. An exothermic peak was also observed at the same temperature range of the second mass loss event [6, 7]. The exothermic peak, attributed to magnetite formation, was shifted to lower temperatures with the addition of manganese and copper to iron oxide, indicating that the metal ions in the iron oxide precursor promote the formation of magnetite phase at lower temperatures [7]. For FCN sample, a small exothermic peak was observed at DTA curve, close to 473 K, in addition to higher exothermic peaks (temperature higher than 533 K) present in all curves; the DTG curve (Fig. 2) of the same sample showed two simultaneous

Table 2 Decomposition mechanism of precursors for each mass loss event

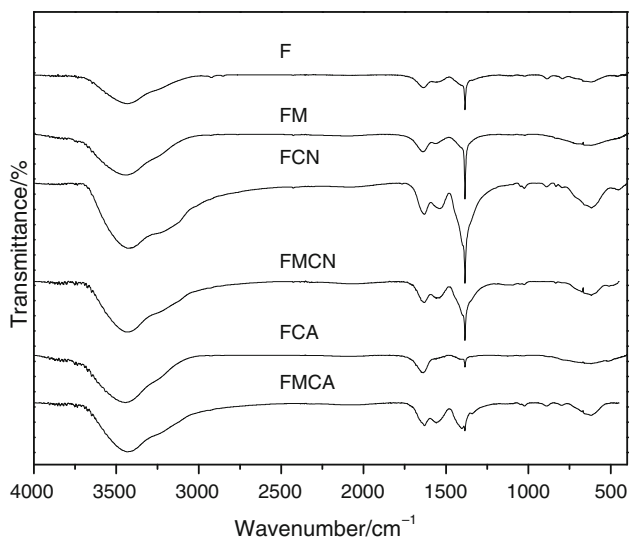
Sample	Rate/°C min ⁻¹	Event	R ²	σ	Model
F	5	1°	0.9999	0.1167	D4
		2°	0.9602	4.29 × 10 ⁻⁷	R3
	10	1°	0.9998	0.1241	D4
		2°	0.9770	4.01 × 10 ⁻⁷	R3
	15	1°	0.9999	0.1146	D4
		2°	0.9780	4.05 × 10 ⁻⁷	R3
FM	5	1°	0.9999	0.1185	D4
		2°	0.9879	4.50 × 10 ⁻⁷	R3
	10	1°	0.9999	0.1106	D4
		2°	0.9900	4.05 × 10 ⁻⁷	R3
	15	1°	0.9990	0.1828	D4
		2°	0.9305	3.30 × 10 ⁻⁷	R3
FCN	5	1°	0.9999	0.1169	D4
		2°	0.9940	4.18 × 10 ⁻⁷	R3
	10	1°	0.9999	0.1255	D4
		2°	0.9879	4.09 × 10 ⁻⁷	R3
	15	1°	0.9999	0.1299	D4
		2°	0.9841	3.61 × 10 ⁻⁷	R3
FMCN	5	1°	0.9998	0.1341	D4
		2°	0.9875	3.85 × 10 ⁻⁷	R3
	10	1°	0.9999	0.1167	D4
		2°	0.9969	4.18 × 10 ⁻⁷	R3
	15	1°	0.9999	0.1053	D4
		2°	0.9869	4.26 × 10 ⁻⁷	R3
FCA	5	1°	0.9992	0.1409	D4
		2°	0.9914	2.80 × 10 ⁻⁷	R3
	10	1°	0.9992	0.1504	D4
		2°	0.9890	3.09 × 10 ⁻⁷	R3
	15	1°	0.9989	0.147	D4
		2°	0.9958	1.04 × 10 ⁻⁷	R3
FMCA	5	1°	0.9991	0.1591	D4
		2°	0.9875	2.24 × 10 ⁻⁷	R3
	10	1°	0.9998	0.0731	D4
		2°	0.9898	5.04 × 10 ⁻⁷	R3
	15	1°	0.9998	0.1267	D4
		2°	0.9717	3.27 × 10 ⁻⁷	R3

events taking place at the temperature range 473–573 K. A similar phenomenon was observed in the DTA and DTG curves of FMCN sample. This effect may be associated with the presence of nitrate ion, which has not been removed during gel washing, or the presence of acetate species, coordinated in different forms of iron oxide precursor [6, 7].

All DTA curves showed broad low-intensity exothermic peaks at temperatures higher than 773 K. FCN, FMCN, FCA and FMCA sample curves showed broad low-intensity exothermic peaks at 777, 819, 790 and 831 K,

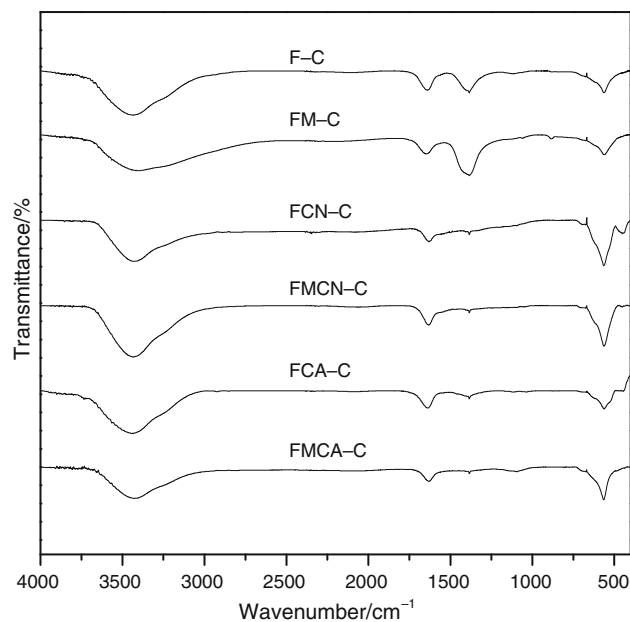
Table 3 Activation energy (E), pre-exponential constant (A), the correlation coefficient (R^2) and standard deviation (σ) obtained by Ozawa and Kissinger method

Sample	Event	Ozawa method				Kissinger method			
		$E/\text{kJ mol}^{-1}$	A/s^{-1}	R^2	σ	$E/\text{kJ mol}^{-1}$	A/s^{-1}	R^2	σ
F	1°	59.97	4.08×10^{-3}	0.9391	0.05	57.38	1.74×10^5	0.9131	0.05
	2°	51.06	$5.04 \times 10^{+4}$	0.8954	0.06	42.02	2.63×10^{-2}	0.8519	0.06
FM	1°	108.11	$6.71 \times 10^{+18}$	0.7250	0.03	102.60	7.40×10^{12}	0.7036	0.03
	2°	243.22	$6.63 \times 10^{+22}$	0.9279	0.01	234.28	3.03×10^{16}	0.9227	0.38
FCN	1°	54.58	$1.77 \times 10^{+8}$	0.8708	0.06	48.98	2.22×10^{-2}	0.8444	0.06
	2°	42.45	$1.60 \times 10^{+4}$	0.9583	0.07	33.97	9.76×10^{-3}	0.9356	0.01
FMCN	1°	34.98	$2.16 \times 10^{+5}$	0.8665	0.09	29.32	2.84×10^{-1}	0.8193	0.09
	2°	35.85	$4.86 \times 10^{+3}$	0.9220	0.09	27.56	3.24×10^{-3}	0.9863	0.09
FCA	1°	123.75	$7.63 \times 10^{+18}$	0.7798	0.02	118.20	9.16×10^{12}	0.7635	0.02
	2°	92.95	$1.74 \times 10^{+18}$	0.8801	0.03	83.66	7.86×10^{-1}	0.8557	0.03
FMCA	1°	124.89	$8.14 \times 10^{+18}$	0.7467	0.02	119.30	9.63×10^{12}	0.7289	0.02
	2°	18.17	$1.22 \times 10^{+2}$	0.9970	0.18	9.77	1.12×10^{-4}	0.9887	0.18

**Fig. 3** Precursor FTIR spectra

respectively. The FM precursor curve showed a similar peak at 863 K followed by a mass loss event. These peaks can be attributed to iron oxide phase changes [6, 7].

Thermogravimetric analysis (TG) was used to investigate the precursor thermal decomposition mechanism through experiments at 278, 283 and 288 K min⁻¹ heating rates. From TG curve data, several solid thermal decomposition kinetic equation models were tested by applying the equation proposed by Coats–Redfern [8]. The kinetic model chosen to represent each event of the decomposition process was the one which provided the linear correlation coefficient closest to unit and the lowest standard deviation (Table 2). Based on the results, it can be inferred that at

**Fig. 4** Doped iron oxide FTIR spectra

temperatures lower than 473 K, corresponding to dehydration/dehydroxylation process, the reaction rate is controlled by diffusion processes according to the three-dimensional diffusion model (D4). Additionally, at 473–573 K temperature range, second mass loss stage (corresponding to magnetite formation) the model that best fit was the three-dimensional nuclear growth geometric model (R3). This model is typical of materials with spherical geometry in which the reaction rate varies with the geometry and particle size. These results show that the precursor decomposition kinetics, producing reducing

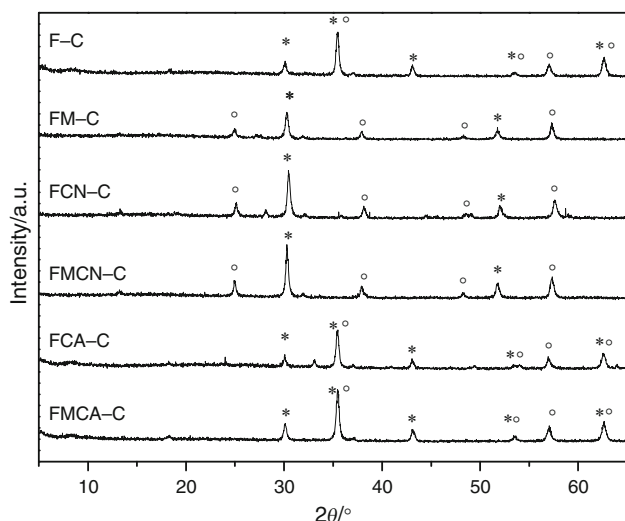


Fig. 5 XRD pattern for doped iron oxides [magnetite (*asterisk symbol*) and hematite (*degree symbol*)]

Table 4 Specific area (S), pore diameter (D_p), pore volume (V_p) and pore size distribution of the oxides

Sample	$S_{\text{BET}}/\text{m}^2 \text{ g}^{-1}$	D_p/nm	$V_p/\text{cm}^3 \text{ g}^{-1}$
F-C	23	37	0.13
FM-C	38	25	0.17
FCN-C	14	37	0.08
FMCN-C	35	37	0.21
FCA-C	21	26	0.10
FMCA-C	31	48	0.22

species which lead to Fe(II) formation from Fe(III) reduction, depends on the solid morphological characteristics.

Kinetic decomposition parameters (activation energy and pre-exponential factor) were determined by using Ozawa and Kissinger methods [8–10]. According to Ozawa's method, these parameters can be obtained by linear regression of Eq. 1 by plotting graph $\ln\beta$ versus $1/T_m$. Kissinger's method admits that the kinetic parameters can be obtained by linear regression of Eq. 2 by plotting graph $\ln(\beta/T_m^2)$ versus $1/T_m$, where β is the heating rate, R is the gas constant, E_a is the activation energy, and T_m is the maximum temperature of each mass loss event obtained by DTG curves (Fig. 2).

$$\ln\beta = (E_a/RT_m) + \ln A \quad (1)$$

$$\ln\left(\frac{\beta}{T_m^2}\right) = (-E_a/RT_m) + \ln(AR/E_a) \quad (2)$$

The activation energy values obtained by both methods are similar to each other (Table 3). The decomposition

processes of F, FCN and FMCN samples, evidenced in the first mass loss event, showed activation energy values close and far lower than those observed by analyzing FM, FCA and FMCA samples. This result indicates that in the second sample group, the hydroxyl is more strongly coordinated in the iron oxide precursor structure [9]. The activation energies of the second loss mass event of F, FCN and FMCN samples are relatively close considering the approximations. FM and FMCA samples were, respectively, those who had the highest and the lowest activation energy value in the second mass loss event. These results indicate that the dopants do not influence the decomposition mechanism, as seen in Table 2, but alter the kinetics of the process.

The thermoanalytical studies have been complemented by FTIR material characterization (oxides and precursors), powder XRD, textural characterization and TPR (oxides).

Precursor infrared spectra (Fig. 3) showed a broad band at 3440 cm^{-1} assigned to OH bonds stretching vibrations of water molecules [9, 11]. At 1540 and 1430 cm^{-1} , bands can be observed assigned to carboxylate ion asymmetric and symmetric stretching [5, 11]. These results suggest that the acetate ions present in the washing solution was adsorbed on the gel. The calcined sample spectra (Fig. 4) also show a carboxylate ion band, less intense, as a result of decomposition of these species, which is in agreement with TG/DTA precursors study [8, 11].

A band at 1380 cm^{-1} can be observed in all precursor spectra, attributed to nitrate groups, suggesting that the solid rinsing step was not enough for complete ion removal of manganese and copper precursor [5, 12]. For FCA and FMCA solids, samples in which the copper precursor was incorporated by copper acetate, the nitrate band is less intense. Below 800 cm^{-1} , a broad band allocated to Fe–O stretching vibration can be observed [5, 12].

The calcined sample spectra (Fig. 4) demonstrate band decrease at 1380 cm^{-1} , indicating nitrate anion partial removal after calcination. In the same figure, a narrowband observed at 567 cm^{-1} can be attributed to crystalline iron oxide (magnetite) [5].

The crystalline nature of iron oxide was confirmed by XRD. From XRD pattern (Fig. 5) of the solid after calcination, the formation of a phases mixture, magnetite and hematite, can be observed. These results are in agreement with Fe(II)/Fe(III) molar ratio lower than stoichiometric magnetite (0.50).

Magnetite formation on the precursor decomposition containing acetate species is in agreement with the literature as previously discussed, once carbon monoxide and other gases are produced, making a reductive atmosphere and thus favoring the reduction of Fe^{3+} to Fe^{2+} [5].

Table 4 shows the oxide textural properties. It is observed that manganese contributes significantly to the

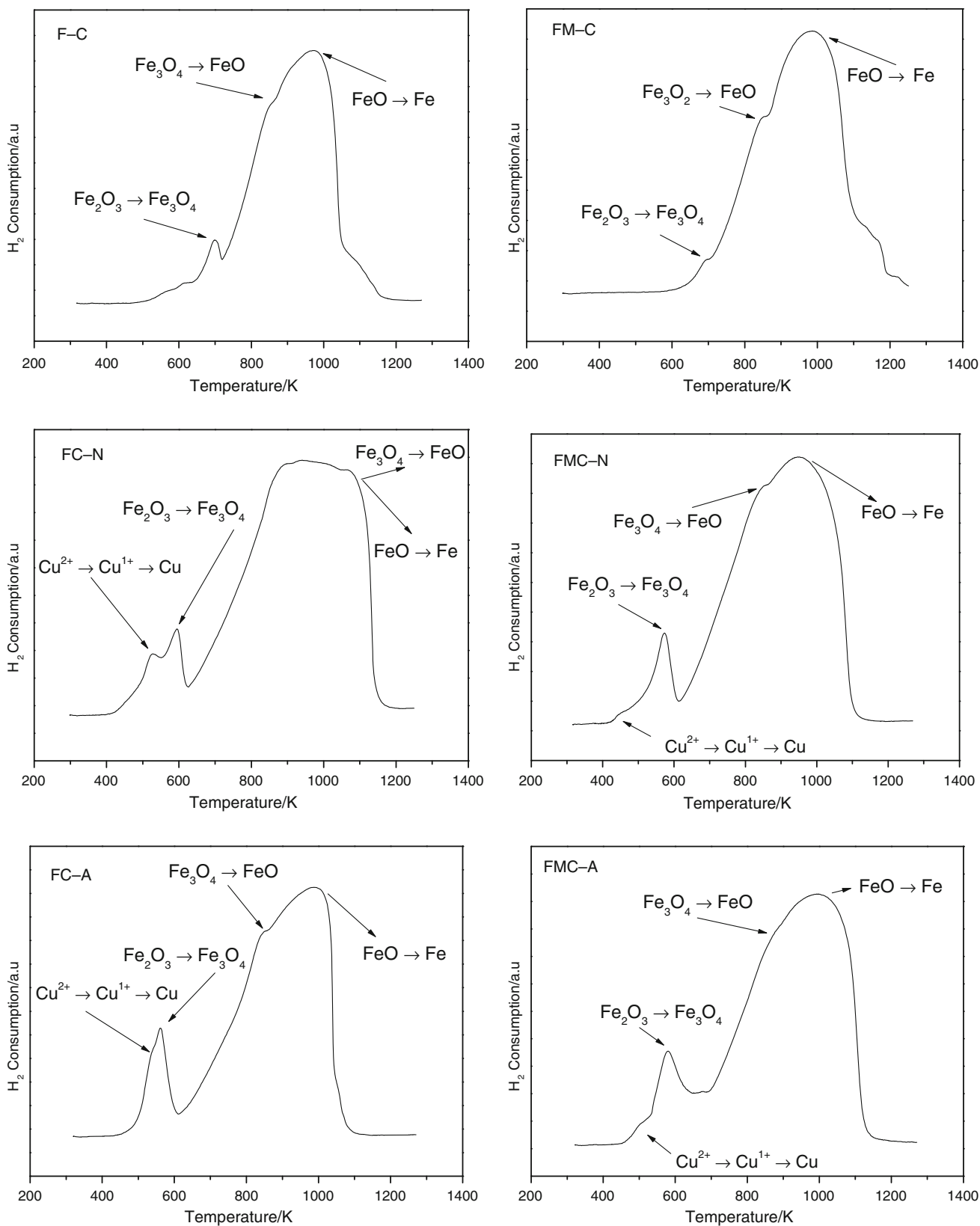


Fig. 6 Thermoprogrammed reduction

Table 5 Temperature corresponding to maximum point of the oxide reduction peaks

Sample	$T_{\max}/^{\circ}\text{C}$ $\text{Fe}_2\text{O}_3 \rightarrow \text{Fe}_3\text{O}_4$	$T_{\max}/^{\circ}\text{C}$ $\text{Fe}_3\text{O}_4 \rightarrow \text{FeO}$	$T_{\max}/^{\circ}\text{C}$ $\text{FeO} \rightarrow \text{Fe}$
F-C	427	578	>693
FM-C	418	575	>712
FCN-C	322	>600	>600
FMCN-C	300	578	>671
FCA-C	290	571	>703
FMCA-C	306	605	>723

increase in iron oxide surface area and pore volume. This result is in agreement with the literature which classifies the dopant as textural promoter [7]. Copper, when added to the system from the impregnation with copper nitrate solution, leads to area decrease, while the area is not significantly affected when the copper acetate precursor is used. This indicates that impregnation with copper acetate solution is the best route for iron oxide doped with copper.

It can also be inferred that the metal synergistic effect (sample FMCN-C) has led to a higher area value, when compared to pure oxide (F-C). On the other hand, the highest Fe(II)/Fe(III) ratio was obtained in the sample only with copper promoter produced from gel impregnation with copper acetate (FCA-C). However, the lower activation energy value in the second decomposition stage corresponding to the reduction of Fe(III) to Fe(II) was observed in the process of precursor decomposition doped with copper and manganese impregnated with copper acetate (FMCA). A possible explanation for this effect can be associated with FCA-C sample lower average diameter and pore volume (Table 4) which may have made it difficult the decomposition gases output, thus increasing the reducing mixture contact time with the sample during calcination.

The complete reduction of hematite to magnetite and magnetite stability regarding wustite (FeO) and metallic iron formation was studied by TPR. In the TPR curves of all samples, the peaks were observed in the range of 523–703 K (Fig. 6) corresponding to reduction of hematite (Fe_2O_3) to magnetite (Fe_3O_4) [7]. Regarding the copper-doped solid curves (FCN-C, FMCN-C, FMCA-C and FCA-C), simultaneous events can be observed in the first process step, with two overlapping peaks (Fig. 6). The first peak occurred at temperatures below 543 K (Fig. 6) and can be related to the reduction of Cu^{2+} to Cu^+ and/or Cu^+ to Cu^0 ; according to the literature, the presence of these species favors the reduction of hematite to magnetite [7, 13–15]. This effect was evidenced by lower reduction temperature from hematite to magnetite with copper-doped solids when compared to the pure iron oxide (sample F-C) and those

doped only with manganese (sample FM-C), as it can be seen from Table 5.

The second reduction step occurs above 843 K in which overlapping peaks can be observed which can be related to magnetite reduction to wustite (FeO) and wustite to metallic iron [7]. The solid FMCA-C showed greater stability, with higher-temperature reduction of magnetite to wustite and wustite to metallic iron (Table 5).

Conclusions

The presence of manganese and copper promoters shifted the precursor decomposition temperature to lower values. For precursor thermal decomposition, according to the model of Coats–Redfern, the dehydration/dehydroxylation step is controlled by diffusion of volatile species; the step related to precursor decomposition with reduction of Fe^{3+} to Fe^{2+} ions is controlled by the particle geometry and size. FCA-C sample showed the highest ratio Fe(II)/Fe(III), indicating that reduction was enhanced for precursor decomposition process. By using Ozawa and Kissinger method, it became clear that the decomposition of precursor FMCA showed the lowest activation energy value leading to FMCA-C solid with higher specific surface area and pore volume than that for iron oxide-free dopants. The referred sample showed easy reduction of hematite to magnetite (low temperature) and the highest stability of magnetite under reductive conditions.

Acknowledgements The authors wish to acknowledge the financial support received from Capes (Coordenação de Aperfeiçoamento de Pessoas de Nível Superior) and Dr. Maria do Carmo Rangel and Dr. Soraia Teixeira Brandão—Universidade Federal da Bahia (UFBA)—for analysis support.

References

- Meshkani F, Rezaei M. Preparation of nanocrystalline metal (Cr, Al, Mn, Ce, Ni, Co and Cu) modified ferrite catalysts for the high temperature water gas shift reaction. *Renew Energy*. 2015;74:588–98.
- Meshkani F, Rezaei M, Jafarbegloo M. Applying Taguchi robust design to the optimization of the synthesis parameters of nanocrystalline Cr-free Fe–Al–Cu catalyst for high temperature water gas shift reaction. *Mater Res Bull*. 2015;70:229–35.
- Leea D, Leea MS, Leea JY, Kima S, Eoma H, Moonc DJ, Leea K. The review of Cr-free Fe-based catalysts for high-temperature water-gas shift reactions. *Catal Today*. 2013;210:2–9.
- Fonseca JSL, Albuquerque RTV, Souza MOG. Catalytic properties of iron oxides impregnated with copper acetate. *React Kinet Catal Lett*. 2007;91:127–30.
- Varela MCR, Filho MFJ, Galembeck F. Effect of acetate on ferrihydrite crystallization. *Hyperfine Interact*. 1994;83:161–7.
- Liang X, Zhong Y, Tan W, Zhu J, Yuan P, He H, Jiang Z. The influence of substituting metals (Ti, V, Cr, Mn, Co and Ni) on the thermal stability of magnetite. *J Therm Anal Calorim*. 2013;111:1317–24.

7. Liang X, Zhong Y, Zhu S, He H, Yuan P, Zhu J, Jiang Z. The valence and site occupancy of substituting metals in magnetite spinel structure $\text{Fe}_{3-x}\text{M}_x\text{O}_4$ ($\text{M} = \text{Cr}, \text{Mn}, \text{Co}$ and Ni) and their influence on thermal stability: an XANES and TG-DSC investigation. *Solid State Sci.* 2013;15:115–22.
8. Muraleedharan K. Thermal decomposition kinetics of potassium iodate. *J Therm Anal Calorim.* 2013;114:491–6.
9. Vergara UL, et al. Polymerization and curing kinetics of furan resins under conventional and microwave heating. *Thermochim Acta.* 2014;581:92–9.
10. Koga N. Ozawa's kinetic method for analyzing thermoanalytical curves. *J Therm Anal Calorim.* 2013;113:1527–41.
11. Keerthana DS, Namratha K, Byrappa K, Yathirajan HS. Facile one-step fabrication of magnetite particles under mild hydrothermal conditions. *J Magn Magn Mater.* 2015;378:551–7.
12. Mozaffari M, Amighian J, Tavakoli R. The effect of yttrium substitution on the magnetic properties of magnetite nanoparticles. *J Magn Magn Mater.* 2015;378:208–12.
13. Ding M, et al. Influence of manganese promoter on co-precipitated Fe–Cu based catalysts for higher alcohols synthesis. *Fuel.* 2013;109:21–7.
14. Jeong D, Subramanian V, Shim J, Jang W, Seo Y, Roh H, Gu JH, Lim YL. High-temperature water gas shift reaction over Fe/Al/Cu oxide based catalysts using simulated waste-derived synthesis gas. *Catal Lett.* 2013;143:438–44.
15. Meshkani F, Rezaei M. A highly active and stable chromium free iron based catalyst for H_2 purification in high temperature water gas shift reaction. *Int J Hydrog Energy.* 2014;39:18302–11.